

Non-degenerate shell-model effective interactions from the Okamoto-Suzuki and Krenciglowa-Kuo iteration methods

Huan Dong¹, T. T. S. Kuo¹ and J. W. Holt²

¹*Department of Physics,
State University New York at Stony Brook
Stony Brook, New York 11794 and*

²*Physik Department, Technische Universität München, D-85747 Garching, Germany*

(Dated: May 2, 2019)

We present calculations of shell-model effective interactions for both degenerate and non-degenerate model spaces using the Krenciglowa-Kuo (KK) and the extended Krenciglowa-Kuo iteration method recently developed by Okamoto, Suzuki *et al.* (EKKO). The starting point is the low-momentum nucleon-nucleon interaction V_{low-k} obtained from the N^3LO chiral two-nucleon interaction. The model spaces spanned by the sd and $sdpf$ shells are both considered. With a solvable model, we show that both the KK and EKKO methods are convenient for deriving the effective interactions for non-degenerate model spaces. The EKKO method is especially desirable in this situation since the vertex function \hat{Z} -box employed therein is well behaved while the corresponding vertex function \hat{Q} -box employed in the Lee-Suzuki (LS) and KK methods may have singularities. The converged shell-model effective interactions given by the EKKO and KK methods are equivalent, although the former method is considerably more efficient. The degenerate sd -shell effective interactions given by the LS method are practically identical to those from the EKKO and KK methods. Results of the sd one-shell and $sdpf$ two-shell calculations for ^{18}O , ^{18}F , ^{19}O and ^{19}F using the EKKO effective interactions are compared, and the importance of the shell-model three-nucleon forces is discussed.

PACS numbers: 21.60.Cs, 21.30.-x, 21.10.-k

I. INTRODUCTION

The nuclear shell model has provided a very successful framework for describing the properties of a wide range of nuclei. This framework is basically an effective theory [1–3], corresponding to reducing the full-space nuclear many-body problem to a model-space one with effective Hamiltonian $PH_{eff}P = PH_0P + PV_{eff}P$, where H_0 is the single-particle (s.p.) Hamiltonian and P represents the projection operator for the model space which is usually chosen to be a small shell-model space such as the sd shell outside of an ^{16}O closed core. The effective interaction V_{eff} plays a central role in this nuclear shell model approach, and its choice and/or determination have been extensively studied, see e.g. [2–5]. As discussed in these references, V_{eff} may be determined using either an empirical approach where it is required to reproduce selected experimental data or a microscopic one where V_{eff} is derived from realistic nucleon-nucleon (NN) interactions using many-body methods. The folded-diagram theory [1–3] is a commonly used such method for the latter. Briefly speaking, in this theory V_{eff} is given as a folded-diagram series [1–3, 6]

$$V_{eff} = \hat{Q} - \hat{Q}' \int \hat{Q} + \hat{Q}' \int \hat{Q} \int \hat{Q} - \hat{Q}' \int \hat{Q} \int \hat{Q} \int \hat{Q} \cdots, \quad (1)$$

where \hat{Q} represents a so-called \hat{Q} -box, which may be written as

$$\hat{Q}(\omega) = [PVP + PVQ \frac{1}{\omega - HQ} QVP]_L. \quad (2)$$

Here V represents the NN interaction and ω is the so-called starting energy which will be explained later (section II). Thus from the NN interaction V we can in principle calculate the \hat{Q} -box and thereby the effective interaction V_{eff} . Note that we use Q , without hat, to denote the Q -space projection operator. ($P + Q = 1$.) Note also that the \hat{Q} -box is an irreducible vertex function where the intermediate states between any two vertices must belong to the Q space. As indicated by the subscript L in eq. (2), the \hat{Q} -box contains valence linked diagrams only, such as the 1st- and 2nd-order \hat{Q} -box diagrams for ^{18}O and ^{18}F shown in Fig. 1. The \hat{Q}' -box of eq. (1) is defined as $(\hat{Q} - PVP)$, namely \hat{Q}' begins with diagrams 2nd-order in V . The above folded-diagram formalism has been employed in microscopic derivations of shell model effective interactions for a wide range of nuclei [2, 3].

In the present work we would like to explore an extension of the well-known methods for computing the folded diagram series in eq. (1). The Lee-Suzuki (LS) [7–9] iteration scheme has been commonly used in previous microscopic calculations of shell model effective interactions [2, 3]. Here we would like to employ two different methods, the Krenciglowa-Kuo (KK) iteration method [10, 11] and the newly developed extended Krenciglowa-Kuo iteration method of Okamoto, Suzuki, Kumagai and Fujii (EKKO)[12], mainly for the purpose of calculating the shell-model effective interactions for non-degenerate model spaces. As we shall discuss later, it is not convenient to use the LS method for calculating the effective interactions for non-degenerate model spaces such as the $sdpf$ two-shell case, while both the EKKO and the KK

methods can be conveniently applied in this situation. The EKKO method has an additional advantage. When the P - and Q -space are not adequately separated from each other, the \hat{Q} -box employed in the KK method may have singularities, causing difficulty for its iterative solution. An essential and interesting difference between the EKKO and KK methods is that the EKKO method employs the vertex function \hat{Z} -box (to be defined in section II) while in the latter the vertex function \hat{Q} -box is used. This simple replacement (of \hat{Q} by \hat{Z}) has an important advantage in circumventing the singularities mentioned above. As we shall discuss later, both the EKKO and KK methods may provide a suitable framework for calculating shell-model effective interactions for large non-degenerate model spaces which may be needed for describing exotic nuclei with large neutron excess.

The organization of the present paper is as follows. In section II we shall describe a non-degenerate version of the EKKO method [12] and how we apply it and the KK method [10, 11] to shell-model effective interactions. A comparison of these two methods with the LS scheme [7, 8] will be made. Our results will be presented and discussed in section III. We shall first perform a sequence of model calculations comparing the EKKO, KK and LS iteration methods for both degenerate and non-degenerate model spaces. The use of the EKKO and KK methods in calculating the effective interactions for non-degenerate model spaces will be emphasized. Starting from the V_{low-k} interaction [3, 14–16] derived from the chiral N^3LO potential [17], the LS, KK and EKKO methods will all be used to calculate the degenerate sd one-shell effective interactions, a main purpose being to check if the results given by the commonly used LS method agree with the KK and EKKO ones. The KK and EKKO methods will then be employed to calculate the non-degenerate $sdpf$ two-shell effective interactions. The matrix elements of the above degenerate and non-degenerate interactions will be compared. The low-energy spectra of ^{18}O , ^{18}F , ^{19}O and ^{19}F given by these interactions will be discussed. A summary and conclusion will be presented in section IV.

II. FORMALISM

In this section, we shall describe and discuss the KK [10, 11] and the EKKO [12] iteration methods and their application to microscopic calculations of shell-model effective interactions. These methods, to our knowledge, have not yet been employed in such calculations. Let us begin with a brief review of the LS [7, 8] and KK iteration methods. Consider first the degenerate LS method where the model space is degenerate, namely $PH_0P = W_0$, W_0 being a constant. In terms of the \hat{Q} -box of Eq.(2), the effective interactions R_n are calculated iteratively by [7, 8]

$$R_1 = \hat{Q}(W_0), \quad (3)$$

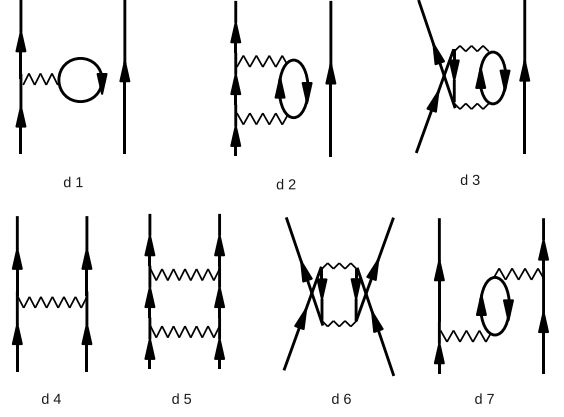


FIG. 1: Low-order diagrams constituting the \hat{Q} -box.

$$R_2 = \frac{1}{1 - \hat{Q}_1} \hat{Q}(W_0), \quad (4)$$

and for $n > 2$

$$R_n = \frac{1}{1 - \hat{Q}_1 - \sum_{m=2}^{n-1} \hat{Q}_m \prod_{k=n-m+1}^{n-1} R_k} \hat{Q}(W_0), \quad (5)$$

where \hat{Q}_m is proportional to the m th derivative of \hat{Q} :

$$\hat{Q}_m = \left. \frac{1}{m!} \frac{d^m \hat{Q}}{d\omega^m} \right|_{\omega=W_0}. \quad (6)$$

The effective interaction is given by the converged R_n , namely

$$V_{eff} = R_{n+1} = R_n. \quad (7)$$

There is a practical difficulty for the above iteration method. In actual shell-model calculations, it is usually not possible to calculate the vertex function \hat{Q} -box exactly; thus it is a common practice to evaluate it with some low-order approximation and calculate the derivatives \hat{Q}_m numerically. At higher orders this becomes increasingly difficult, and therefore such calculations are usually limited to low orders in the iteration. However, as we shall demonstrate in section IIIa, low-order LS iterations are often not accurate when the P - and Q -spaces are strongly coupled.

The above degenerate LS iteration method can be generalized to a non-degenerate one [9], namely PH_0P being non-degenerate. In this situation we need not only the \hat{Q} -box of eq. (2) but also a generalized \hat{Q} -box defined by

$$\hat{Q}_n(\epsilon_1 \epsilon_2 \cdots \epsilon_{n+1}) = (-1)^n [P V Q g_1^Q g_2^Q \cdots g_{n+1}^Q Q V P]_L. \quad (8)$$

with

$$g_i^Q \equiv \frac{1}{\epsilon_i - Q H Q}. \quad (9)$$

This generalized \hat{Q} -box is defined for $n \geq 1$, and ϵ_i is defined by $PH_0P\phi_i = \epsilon_i\phi_i$ where $P = \sum_{m \leq d} |\phi_m\rangle\langle\phi_m|$.

The dimension of the P -space is labelled d . Note that only valence-linked diagrams are retained in $\hat{Q}_n(\epsilon_1 \cdots \epsilon_{n+1})$, as indicated by the subscript L.

With the above definitions, the effective interaction given by the non-degenerate LS iteration method is given as [9]

$$\begin{aligned} R_1 &= \sum_{\alpha} \hat{Q}(\epsilon_{\alpha}) P_{\alpha}, \\ R_2 &= \sum_{\alpha} \left[1 - \sum_{\beta} \hat{Q}_1(\epsilon_{\alpha\beta}) P_{\beta} \right]^{-1} \hat{Q}(\epsilon_{\alpha}) P_{\alpha}, \\ R_3 &= \sum_{\alpha} \left[1 - \sum_{\beta} \hat{Q}_1(\epsilon_{\alpha\beta}) P_{\beta} - \sum_{\beta\gamma} \hat{Q}_2(\epsilon_{\alpha\beta\gamma}) P_{\beta} R_2 P_{\gamma} \right]^{-1} \\ &\quad \times \hat{Q}(\epsilon_{\alpha}) P_{\alpha}, \\ &\dots \end{aligned}$$

with $\epsilon_{\alpha\beta} \equiv (\epsilon_{\alpha} + \epsilon_{\beta})$, $\epsilon_{\alpha\beta\gamma} \equiv (\epsilon_{\alpha} + \epsilon_{\beta} + \epsilon_{\gamma})$, \dots . In the above equations $P_m = |\phi_m\rangle\langle\phi_m|$. When convergent, we have $V_{eff} = R_{n+1} = R_n$. The above non-degenerate LS method can be used to calculate the effective interactions for e.g., the non-degenerate $0p$ -shell [13] or the two-shell *sd**pf* model space. But this method is rather complicated for computations, and this has hindered its application to microscopic calculations of shell-model effective interactions.

We now describe some details of the non-degenerate KK and EKKO methods. The KK iteration method was originally developed for model spaces which are degenerate [10]. A non-degenerate KK iteration method was later formulated [11], with the effective interaction given by the following iteration methods. Let the effective interaction for the i th iteration be $V_{eff}^{(i)}$ and the corresponding eigenvalues E and eigenfunctions χ be given by

$$[PH_0P + V_{eff}^{(i)}]\chi_m^{(i)} = E_m^{(i)}\chi_m^{(i)}. \quad (11)$$

Here χ_m is the P -space projection of the full-space eigenfunction Ψ_m , namely $\chi_m = P\Psi_m$. The effective interaction for the next iteration is then

$$V_{eff}^{(i+1)} = \sum_m [PH_0P + \hat{Q}(E_m^{(i)})] |\chi_m^{(i)}\rangle\langle\tilde{\chi}_m^{(i)}| - PH_0P, \quad (12)$$

where the bi-orthogonal states are defined by

$$\langle\tilde{\chi}_m|\chi_{m'}\rangle = \delta_{m,m'}. \quad (13)$$

Note that in the above PH_0P is non-degenerate. The converged eigenvalue E_m and eigenfunction χ_m satisfy the P -space self-consistent condition

$$(E_m(\omega) - H_0)\chi_m = \hat{Q}(\omega)\chi_m, \quad \omega = E_m(\omega). \quad (14)$$

To start the iteration, we use

$$V_{eff}^{(1)} = \hat{Q}(\omega_0) \quad (15)$$

where ω_0 is a starting energy chosen to be close to PH_0P . The converged KK effective interaction is given by $V_{eff} = V_{eff}^{(n+1)} = V_{eff}^{(n)}$. When convergent, the resultant V_{eff} is independent of ω_0 , as it is the states with maximum P -space overlaps which are selected by the KK method [10]. We shall discuss this feature later in section III using a solvable model. The above non-degenerate KK method is numerically more convenient than the non-degenerate LS method.

The diagrams of Fig. 1 have both one-body (d1,d2,d3) and two-body (d4,d5,d6,d7) diagrams. When we calculate nuclei with two valence nucleons such as ^{18}O and ^{18}F , all seven diagrams are included in the \hat{Q} -box. But for nuclei with one valence nucleon such as ^{17}O , we deal with the 1-body \hat{S} -box which is approximated by the sum of diagrams d1, d2 and d3. The 1-body effective interaction is given by a similar KK iteration

$$S_{eff}^{(i+1)} = \sum_m [PH_0P + \hat{S}(E_m^{(i)})] |\chi_m^{(i)}\rangle\langle\tilde{\chi}_m^{(i)}| - PH_0P. \quad (16)$$

Denoting its converged value as S_{eff} , the model-space s.p. energy ϵ_m^{eff} is given by $P_m(H_0 + S_{eff})P_m$. By adding and then subtracting S_{eff} , we can rewrite Eq.(14) as

$$(E_m(\omega) - H_0^{eff})\chi_m = [\hat{Q}(\omega) - S_{eff}]\chi_m, \quad \omega = E_m(\omega), \quad (17)$$

with $H_0^{eff} = H_0 + S_{eff}$. In most shell model calculations [4, 5], one often uses the experimental s.p. energies. This treatment for the s.p. energies is in line with the above subtraction procedure, as $P(H_0 + S_{eff})P$ represents the physical s.p. energy which in principle can be extracted from experiments. In the present work we shall use the experimental s.p. energies for the model-space orbits together with the V_{eff} derived from $(\hat{Q} - S_{eff})$. A similar subtraction procedure has also been employed in the LS calculations [2, 3] where the all-order sum of the one-body diagrams was subtracted from the calculation of the effective interaction.

In several aspects, the above KK method provides a more desirable framework for effective interaction calculations than the commonly used LS method. The KK method is more convenient for non-degenerate model spaces than the LS method, and the KK method does not require the calculation of high-order derivatives of the \hat{Q} -box, which may be necessary in a converged LS calculation. The KK method has, however, a shortcoming when applied to calculations with extended model space such as the two-shell *sd**pf* one. For example, certain 2nd-order diagrams for this case may diverge, resulting in an ill-defined \hat{Q} -box. It is remarkable that these potential divergences can be circumvented by the recently proposed EKKO method of Okamoto et al. [12]. In this method, the vertex function \hat{Z} -box is employed. It is related to the \hat{Q} -box by

$$\hat{Z}(\omega) = \frac{1}{1 - \hat{Q}_1(\omega)} [\hat{Q}(\omega) - \hat{Q}_1(\omega)P(\omega - H_0)P], \quad (18)$$

where \hat{Q}_1 is the first-order derivative of the \hat{Q} -box. The \hat{Z} -box considered by Okamoto *et al.* [12] is for degenerate model spaces ($PH_0P = W_0$), while we consider here a more general case with non-degenerate PH_0P . An important property of the above \hat{Z} -box is that it is finite when the \hat{Q} -box is singular (has poles). Note that $Z(\omega)$ satisfies

$$\hat{Z}(\omega)\chi_m = \hat{Q}(\omega)\chi_m \text{ at } \omega = E_m(\omega). \quad (19)$$

The iteration method for determining the effective interaction from the \hat{Z} -box is quite similar to that for the \hat{Q} -box. Suppose the effective interaction for the i th iteration is $V_{eff-Z}^{(i)}$. The corresponding eigenfunction χ and eigenvalues E^Z are determined by

$$[PH_0P + V_{eff-Z}^{(i)}]\chi_m^{(i)} = E_m^{Z(i)}\chi_m^{(i)}. \quad (20)$$

The effective interaction for the next iteration is

$$V_{eff-Z}^{(i+1)} = \sum_m [PH_0P + \hat{Z}(E_m^{Z(i)})][\chi_m^{(i)}\langle\chi_m^{(i)}| - PH_0P, \quad (21)$$

Although $\hat{Q}(\omega)$ and $\hat{Z}(\omega)$ are generally different, it is interesting that the converged eigenvalues E_m of $P(H_0 + V_{eff})P$ and the corresponding ones E_m^Z of $P(H_0 + V_{eff-Z})P$ are both exact eigenvalues of the full-space Hamiltonian $H = H_0 + V$, which can be seen from eqs. (14), (18) and (19). Note, however, the KK and EKKO methods may reproduce different eigenvalues of the full-space Hamiltonian H . This aspect together with some other comparisons of these methods will be discussed in section IIIa, using a simple solvable model.

For the degenerate case, Okamoto *et al.* [12] have shown that $\frac{dE_m^Z(\omega)}{d\omega} = 0$ at the self-consistent point $\omega = E_m^Z(\omega)$. As outlined below, we have found that this result also holds for the case of non-degenerate PH_0P . From eq. (18), we have

$$\frac{dZ}{d\omega} = \frac{2}{1 - \hat{Q}_1} \hat{Q}_2 \frac{1}{1 - \hat{Q}_1} [\hat{Q} - \hat{Q}_1(\omega - H_0)] - \frac{2}{1 - \hat{Q}_1} \hat{Q}_2(\omega - H_0). \quad (22)$$

Then from eqs. (14) and (19) we have

$$\left[\frac{dZ(\omega)}{d\omega}\right]_{\omega=E_m^Z}|\chi_m\rangle = 0, \quad (23)$$

and

$$\left[\frac{dE_m^Z(\omega)}{d\omega}\right]_{\omega=E_m^Z} = 0. \quad (24)$$

This is a useful result; it states that at any self-consistent point the eigenvalues $E_m^Z(\omega)$ varies ‘flatly’ with ω , a feature certainly helpful to iterative calculations. In section III, we shall check this feature numerically.

III. RESULTS AND DISCUSSION

IIIa. Model calculations comparing the LS, KK and EKKO methods

In this section we shall study the above iteration methods by way of a simple matrix model, similar to the one employed in [12]. We consider a 4-dimensional matrix Hamiltonian $H = H_0 + H_1$ where

$$H_0 = \begin{bmatrix} PH_0P & 0 \\ 0 & QH_0Q \end{bmatrix} \quad (25)$$

and

$$PH_0P = \begin{bmatrix} \varepsilon_{p1} & 0 \\ 0 & \varepsilon_{p2} \end{bmatrix}; \quad QH_0Q = \begin{bmatrix} \varepsilon_{q1} & 0 \\ 0 & \varepsilon_{q2} \end{bmatrix}. \quad (26)$$

The interaction Hamiltonian has a strength parameter x , namely

$$H_1 = \begin{bmatrix} PH_1P & PH_1Q \\ QH_1P & QH_1Q \end{bmatrix}, \quad (27)$$

with

$$\begin{aligned} PH_1P &= \begin{bmatrix} 0 & 5x \\ 5x & 10x \end{bmatrix}; \\ PH_1Q &= QH_1P = \begin{bmatrix} 0 & 8x \\ 8x & 0 \end{bmatrix}; \\ QH_1Q &= \begin{bmatrix} -5x & x \\ x & -5x \end{bmatrix}. \end{aligned} \quad (28)$$

As discussed in section II, both the KK and EKKO iteration methods are rather convenient for non-degenerate model spaces. We would like to check this feature by carrying out some calculations using the above model. We consider two unperturbed Hamiltonians, given by $(\varepsilon_{p1}, \varepsilon_{p2}, \varepsilon_{q1}, \varepsilon_{q2}) = (0, 6, 4, 9)$ and $(0, 0, 4, 9)$. The PH_0P parts of them are, respectively, non-degenerate and degenerate.

In the first three entries of Table I, some results for the $PH_0P = (0, 6)$ case are presented. Here E_n are the exact eigenvalues of the full Hamiltonian, with their model-space overlaps denoted by $\langle n|P|n\rangle$. The entries E_{KK} and E_{EKKO} are the eigenvalues generated respectively by the KK and EKKO iteration methods. Not only is the above PH_0P non-degenerate but its spectrum intersects that of QH_0Q . One would expect that this PH_0P may cause difficulty for the above iteration methods. But as indicated in Table I, both the non-degenerate KK and the non-degenerate EKKO iteration methods work remarkably well. Note that the interaction used here is rather strong ($x=0.6$), and both methods still work well, converging to values of E_n which are quite far from PH_0P .

Some results for the degenerate case of $PH_0P = (0, 0)$ are listed in the last two entries of Table I. Here we have performed calculations using the degenerate LS method through 5th order iteration (i.e. in Eq.(7) we use

$V_{eff} = R_5$). As shown, the results so obtained are not in good agreement with the exact results. This suggests that low-order LS iteration method may often be inadequate, and one needs higher-order iterations to obtain accurate results.

It is known that the KK iteration method converges to the states with maximum P -space overlaps [10], while the LS method converges to the states of lowest energies [7, 8]. We have found that for many cases the EKKO method also converges to states of maximum P -space overlaps. As listed in the third entry of Table I, both the KK and EKKO methods converge to states of energies $E_n = -3.51$ and 14.53 whose P -space probabilities are relatively 0.70 and 0.86 . We have also found that the EKKO and KK iteration methods can converge to different states. An example is the result shown in the last part of Table I, where the EKKO method converges to states of energy (P -space probability) -1.45 (0.87) and 0.91 (0.46), while the states of maximum P -space overlap are those with energies -1.45 and 5.25 . Note that for this case the EKKO method is clearly more accurate than the KK method.

We have noticed that for a number of cases the EKKO method converges well but not so for the KK method. This is largely because these two methods treat the singularities of the \hat{Q} -box differently. To see this, let us perform a graphical solution for the $x=0.60$ case of Table I. Using the parameters of this case, we calculate and plot in Fig. 3 both $E_m^Q(\omega)$ and $E_m^Z(\omega)$ which are respectively the eigenvalues of $P[H_0 + \hat{Q}(\omega)]P$ and $P[H_0 + \hat{Z}(\omega)]P$. As discussed in section II, they have identical self-consistent solutions, namely $\omega = E_m^Q(\omega) = E_m^Z(\omega) \equiv E_m$ where E_m is the eigenvalue of the full-space Hamiltonian. Recall that \hat{Q} and \hat{Z} are given respectively by eqs. (2) and (18). As shown in the figure, the curves of E^Q and E^Z do have identical self-consistent solutions as marked by the common intersection points E_1 , E_2 , E_3 and E_4 . Note that the above two curves are distinctly different from each other, particularly in the vicinity of the poles (marked by the vertical lines through F_1 and F_2) of the \hat{Q} -box. There $E^Q(\omega)$ is discontinuous, diverging oppositely before and after the pole, while $E^Z(\omega)$ remains continuous throughout. This clearly helps the convergence of the \hat{Z} -box iteration method: The \hat{Z} -box iteration proceeds along a continuous $E^Z(\omega)$ curve, while the \hat{Q} -box iteration often does not converge as it may bounce back and forth across the discontinuity.

As seen from eq. (18), the \hat{Z} -box method has ‘false’ solutions at $E_q^Z(\omega) = \omega = \mu_q \equiv F_q$, where μ_q are poles of the \hat{Q} -box. These solutions are marked in Fig. 3 as F_1 and F_2 . These false solutions can be readily recognized and discarded. As given in Eq.(24), we have at self-consistent points $\frac{dE_m^Z}{d\omega} = 0$. As shown in Fig. 3, the slopes of E^Z do satisfy the above condition at the self-consistent points E_1 to E_4 , but not so at the false points F_1 and F_2 .

TABLE I: Results of model calculations using the LS, KK and EKKO iteration methods. See text for other explanations.

$H_0 = (0,6,4,9) \quad x=0.10$					
E_n	-0.110705	3.328164	7.203243	8.579299	
$(n P n)$	0.991108	0.044558	0.953368	0.010966	
E_{KK}	-0.110705	7.203243			
E_{EKKO}	-0.110705	7.203242			
$x=0.30$					
E_n	-0.974184	1.808716	8.080888	10.084581	
$(n P n)$	0.906155	0.111257	0.113523	0.869066	
E_{KK}	-0.974185	10.084580			
E_{EKKO}	-0.974185	10.084581			
$x=0.60$					
E_n	-3.510377	-0.286183	8.265089	14.531471	
$(n P n)$	0.709531	0.189318	0.232422	0.868729	
E_{KK}	-3.510377	14.531472			
E_{EKKO}	-3.510363	14.531472			
$H_0=(0,0,4,9) \quad x=0.10$					
E_n	-0.296201	0.982861	3.736229	8.577111	
$(n P n)$	0.985416	0.922993	0.082811	0.008780	
E_{LS}	-0.314591	0.872176			
E_{KK}	-0.296201	0.982860			
E_{EKKO}	-0.296201	0.982860			
$x=0.30$					
E_n	-1.448782	0.906504	5.254129	8.288149	
$(n P n)$	0.868986	0.460296	0.566014	0.104704	
E_{LS}	-1.620734	0.339561			
E_{KK}	-1.125579	5.515468			
E_{EKKO}	-1.448782	0.906504			

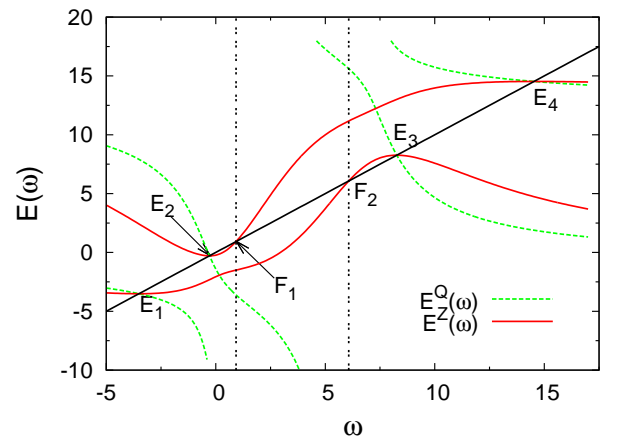


FIG. 2: Graphical solutions for the \hat{Q} - and \hat{Z} -box self-consistent equations. See text for other explanations.

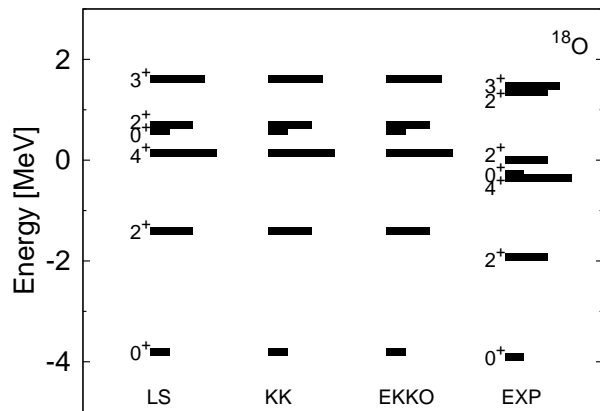


FIG. 3: Energy spectrum of ^{18}O obtained from the sd -shell calculations using the LS, KK and EKKO methods. See text for more explanations.

IIIb. The sd and $sdpf$ shell model effective interactions

In this subsection, we shall calculate the effective interactions for both the degenerate sd one-shell and the non-degenerate $sdpf$ two-shell cases. Before presenting our results, let us first describe some details of our calculations. The LS, KK and EKKO methods as described in section II will be employed. We first compute the low-momentum nucleon-nucleon interaction V_{low-k}^{2N} [3, 14–16] starting from the chiral N^3LO two-body potential [17] at a decimation scale of $\Lambda = 2.1 \text{ fm}^{-1}$. At this cutoff scale, the low-momentum interactions derived from different NN potentials [17–20] are remarkably close to each other, leading to a nearly unique low-momentum interaction [16]. The effect of the leading-order chiral three-nucleon force on shell model effective interactions has been studied, and our results will be reported in a separate publication [21]. The above V_{low-k}^{2N} interaction is then used in calculating the \hat{Q} -box diagrams as shown in Fig. 1. In calculating these diagrams, the hole orbits are summed over the $0s0p$ shells and particle orbits over the $0d1s1p0f$ shells. The active spaces (P -space) used for the one-shell and two-shell calculations are respectively the three orbits in the sd shell and the seven orbits in the $sdpf$ shells. The experimental s.p. energies of (0.0, 5.08, 0.87) MeV have been used, respectively, for the ($0d_{5/2}, 0d_{3/2}, 1s_{1/2}$) orbits [22]. We have employed the shell-model s.p. wave functions and energies with the harmonic oscillator constant of $\hbar\omega=14 \text{ MeV}$.

In the following, let us first report our results for the degenerate sd one-shell calculations. Here by degenerate we mean that the unperturbed s.p. energy levels for the ($0d_{5/2}, 0d_{3/2}, 1s_{1/2}$) orbits are degenerate. Our purpose here is mainly to compare the results given by the KK and EKKO method with those given by the commonly used degenerate LS method [2, 3]. Our results are pre-

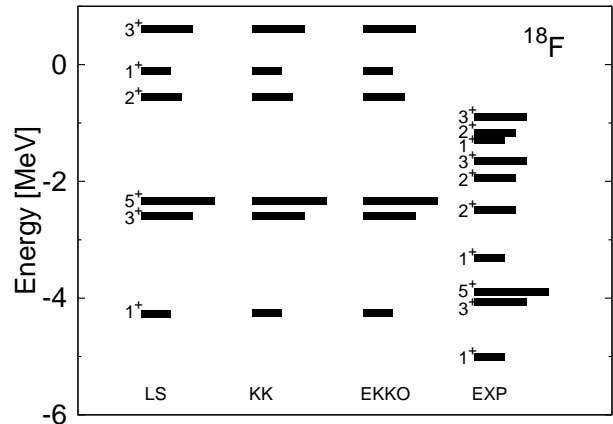


FIG. 4: Same as Fig. 3 except for ^{18}F .

sented in Figs. 3 and 4. As discussed in section II and illustrated in Table I, the EKKO and KK methods may converge to different states. In the present calculations they actually converge to the same states, as seen in Figs. 3 and 4. Our LS calculations are carried out using a low-order approximation, namely we take $V_{eff} = R_5$ (see eq. (7)). As shown in the figures, the LS, KK and EKKO results for both ^{18}O and ^{18}F are in fact nearly identical to each other. A comparison of our results with experiments [22] is also presented in the figures. The agreement between our calculated energy levels with experiments is moderately satisfactory for ^{18}O , but for ^{18}F the calculated lowest ($1^+, 3^+, 5^+$) states, though of correct ordering, are all significantly higher than the experimental values. As discussed in sections II and IIIa, the LS method is known to converge to the states of the lowest energies, while the KK method to the states of maximum P -space overlaps. Thus the good agreement shown in Figs. 3 and 4 is an important indication that the states reproduced by the model-space LS, EKKO and KK effective interaction are likely those of the lowest energies as well as maximum model-space overlaps. In Fig. 5, we compare the entire sd -shell matrix elements given by the LS and EKKO methods; it is remarkable that every individual LS matrix element is practically equal to the corresponding EKKO one. (The matrix elements given by EKKO and KK are also nearly identical.) Recall that our LS matrix elements were obtained with a low-order R_5 iteration, which indicates the rapid convergence of the iteration scheme in the case of sd -shell effective interactions.

As discussed in sections II and IIIa, the EKKO or KK methods are convenient for deriving the effective interactions for non-degenerate model spaces. In the following let us first apply these methods to a relatively simple case, namely the non-degenerate sd one-shell effective interactions. The shell-model s.p. energies for the sd shell are degenerate, but the experimental ones are not. It may be of interest to employ the experimental

EKKO and KK methods. For the sd shell-model calculations, we have employed the experimental s.p. energies for the three sd -shell orbits as mentioned earlier.

For the $sdpf$ shell-model calculations, we need in addition the experimental s.p. energies for the four pf orbits. Their values are, however, not well known. In the present calculation we have placed them all at a separation of one $\hbar\omega$ (14 MeV) above the $d_{5/2}$ level. (As to be reported later (Fig. 11), we shall also use a smaller value for the above separation.) In our calculations we have considered two choices for the unperturbed s.p. energies of the sd model space, a degenerate one and a non-degenerate one (in which the $0d_{3/2}$ and $1s_{1/2}$ orbits are shifted higher in energy compared to the $0d_{5/2}$ orbit as described earlier). We have found that the results are rather similar, and in the following discussion we report only the calculations for the degenerate sd -shell choice.

In Fig. 7 we compare the matrix elements of the $sdpf$ two-shell EKKO interaction with those of the sd one-shell case. Only the matrix elements within the sd shell are shown. We find that the magnitudes of the two-shell matrix elements are generally weaker than the one-shell matrix elements, some differing by as much as 1 MeV. Despite these differences, the resulting spectra for ^{18}O and ^{18}F given by the one-shell and two-shell calculations are nearly equivalent to each other, as illustrated by the two middle columns of Fig. 8. In our present and subsequent calculations we employ a low-order \hat{Q} -box consisting of the 1st- and 2nd-order diagrams of Fig. 1. It is instructive, however, to compare the one- and two-shell calculations when only the leading-order approximation to the \hat{Q} -box is retained. In the two leftmost columns of Fig. 8 we show the spectra of ^{18}F when only the 1st-order \hat{Q} -box diagrams are included. We note that in this case (in contrast to the second-order \hat{Q} -box calculation) the resulting sd ‘1 Shell’ and $sdpf$ ‘2 Shell’ spectra are largely different.

This important observation can be explained as follows. In general, the different sd and $sdpf$ model spaces will result in different effective interactions and associated effective Hamiltonians, which we denote by H_{eff}^1 and H_{eff}^2 . But since the sd model space is a subspace of $sdpf$ model space, H_{eff}^1 and H_{eff}^2 should in principle have common eigenvalues. We would like to check that this requirement is satisfied by our present calculations. As indicated by the two middle columns of Fig. 8, we see that indeed this is the case. In fact among the many states given by the $sdpf$ calculations, it is the ones with the maximum sd -space overlaps which agree with the results given by the sd -shell calculation, which is a physically desirable result. Because of the difference in the model spaces, the renormalization effects for the sd and $sdpf$ effective interactions are different. To bridge these differences, we need to include at least the 2nd-order \hat{Q} -box diagrams (note that the allowed intermediate states of the 2nd-order \hat{Q} -box diagrams are model-

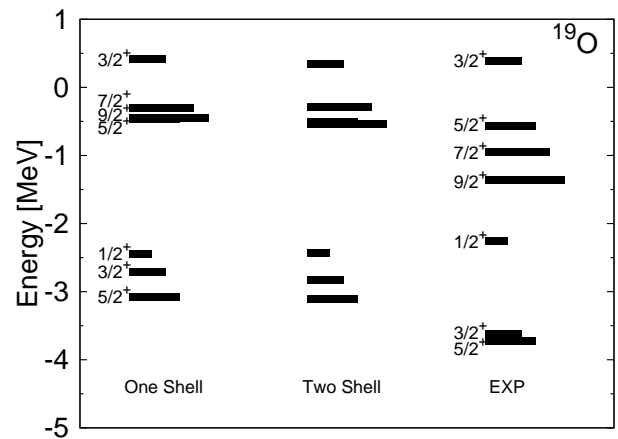


FIG. 9: Low-lying states of ^{19}O calculated with the sd one-shell (1 Shell) and $sdpf$ two-shell (2 Shell) EKKO interactions. The experimental results are from [22].

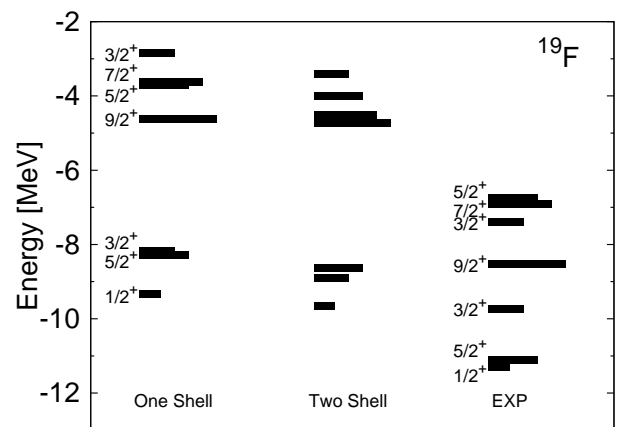


FIG. 10: Same as Fig. 10 except for ^{19}F .

space dependent). These diagrams are not included in the above 1st-order calculations, and consequently the sd and $sdpf$ results are different as shown by the two leftmost columns of Fig. 8, which is a strong evidence for the importance of the model-space-dependent renormalization effects. The construction of model-space effective interactions is in many ways similar to the construction of an effective theory from a renormalization group evolution. In such cases, one would expect that despite the different effective Hamiltonians, the same low-energy physical observables would be reproduced. The shell model effective interactions in the present work have not been computed exactly (that is, including high-order diagrams in the \hat{Q} -box), yet it is interesting that we nevertheless find excellent agreement between the one- and two-shell calculations including \hat{Q} -box diagrams only up to second order.

To further study the sd one-shell and $sdpf$ two-shell effective interactions, we have applied them to shell model calculations of ^{19}O and ^{19}F . The 2nd-order \hat{Q} -box of Fig.

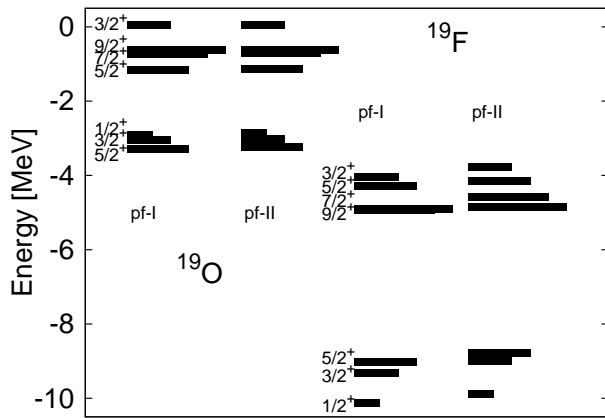


FIG. 11: Low-lying states of ^{19}O and ^{19}F calculated using the *sdpf* two-shell EKKO interactions, with the *pf* experimental s.p. energies placed at 10 ('pf-I') and 14 MeV ('pf-II') above the $0d_{5/2}$ orbit.

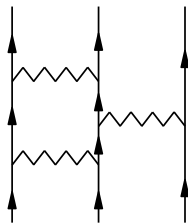


FIG. 12: A shell-model three-nucleon force diagram. Its external lines all belong to the *sd* shell, while its intermediate states between any two vertices must have at least one line belonging to the *pf* shell.

1 is employed. Our results are displayed respectively in Figs. 9 and 10. It is of interest that the one-shell and two-shell results for ^{19}O are nearly identical, and for ^{19}F they are also remarkably close to each other. Although the orderings of our calculated spectra are in fair agreements with experiments, there are significant differences between them. As discussed earlier, in our *sdpf* two-shell calculations the experimental s.p. energies for the four *pf* orbits are needed, but their values are not well known. So far we have chosen to place them at a separation of 14 MeV above the $0d_{5/2}$ orbit. We have repeated our calculations using instead a smaller separation of 10 MeV, to investigate if the use of a smaller separation may improve the agreements. As illustrated in Fig. 11, the low-lying states of ^{19}O are hardly changed, those given by the separations of 14 and 10 MeV being nearly identical. The differences between the two sets of states for ^{19}F are also generally small. That these low-lying states are insensitive to the above separations indicates that our *sdpf* effective interactions (obtained with the inclusion of the 1st- and 2nd-order \hat{Q} -box diagrams of Fig. 1) have a rather weak coupling between the *sd* and *fp* shells.

Recall that we have employed the folded-diagram expansion of eq. (1) to calculate the effective interaction V_{eff} . For nuclei with three valence nucleons, this expansion has both 2-body and 3-body diagrams. (By 3-body diagrams we mean those valence-linked diagrams with three incoming and three outgoing valence lines [1].) As an example, the shell-model three-nucleon force diagram of Fig. 12 should be included in the *sd* one-shell effective interaction for ^{19}O and ^{19}F . But this diagram is not included in our present *sd* one-shell calculation as we employ only the two-body \hat{Q} -box of Fig. 1. This diagram is, however, included in our *sdpf* shell model calculations for ^{19}O and ^{19}F . Thus the good agreement between the one-shell and two-shell results shown in Fig. 9 is an indication that this type of shell-model three-nucleon force is likely to have little importance for ^{19}O spectra, while it is moderately important for ^{19}F as suggested by the small difference shown in Fig. 10. Further studies of this type of three-nucleon force will be useful and of interest, and we plan to do so in a future study.

IV. SUMMARY AND CONCLUSION

We have applied the iteration method of Krenciglowa and Kuo (KK) and that recently developed by Okamoto *et al.* (EKKO) to the microscopic derivation of the *sd* and *sdpf* shell-model effective interactions using the low-momentum nucleon-nucleon interaction derived from the chiral $N^3\text{LO}$ two-body potential. We first considered a solvable model and found that both methods are suitable and efficient for deriving the effective interactions for non-degenerate model spaces, where the Lee-Suzuki iteration method is considerably less convenient. Even in the situation where the *P*- and *Q*-space unperturbed Hamiltonians have spectrum overlaps did the KK and EKKO methods perform remarkably well. The EKKO method has the special advantage that its vertex function \hat{Z} -box is, by construction, a continuous function of the energy, while the \hat{Q} -box function used in the LS and KK methods may have singularities. This feature was found to be particularly useful for the convergence of the EKKO iteration method.

Using the V_{low-k} low-momentum potentials obtained from above two-body interaction, we first calculated the degenerate *sd* one-shell effective interactions using the LS, KK and EKKO methods. The results given by KK and EKKO were found to be identical. It is noteworthy that the LS results, calculated with a low-order (5th order) iteration, were also in very good agreement with both the KK and EKKO results, supporting the accuracy of the low-order LS method for calculating the degenerate shell-model effective interactions.

We have calculated the non-degenerate *sdpf* two-shell effective interactions using both the EKKO and KK methods. Both methods gave identical results and were found to be suitable for such non-degenerate calcula-

tions, with the former being more efficient (faster converging). We have applied these interactions to compute the low-lying energy spectra for several nuclei with two and three valence nucleons above the ^{16}O core. Since the sd model space is a subspace of the $sdpf$ model space, we expect the effective Hamiltonians for these two spaces to have common eigenvalues. Indeed this was largely confirmed in our calculations of ^{18}O , ^{18}F , ^{19}O and ^{19}F spectra, where it was found that the states in the $sdpf$ calculations with the maximum sd -space overlap agreed with the results given by the sd calculations. The above agreement was found to be excellent for ^{19}O , though not as good for ^{19}F , which indicates that the shell-model three-nucleon force is more important in ^{19}F (where the proton-neutron interaction is involved) than in ^{19}O . Further study of this three-nucleon force should be useful and of much interest.

The calculated ground state energies for the above four nuclei are all higher (less bound) than the corresponding experimental values. We are studying if the inclusion of the chiral three-nucleon force may give additional binding energy [21]. In the present work we have employed the \hat{Q} -box irreducible vertex function consisting of the first- and second-order diagrams only. The inclusion of the Kirsan-Babu-Brown (KBB) all-order core polarization diagrams in the \hat{Q} -box may provide additional binding energy [23]. We plan to carry out further calculations with the inclusion of such all-order KBB diagrams.

We are very grateful to L. Coraggio, A. Covello, A. Gargano, Jason Holt, N. Itaco, M. Machleidt, R. Okamoto and K. Suzuki for many helpful discussions. Partial supports from the US Department of Energy under contracts DE-FG02-88ER40388 and the DFG (Deutsche Forschungsgemeinschaft) cluster of excellence: Origin and Structure of the Universe are gratefully acknowledged.

[1] T. T. S. Kuo and E. Osnes, *Lecture Notes in Physics* (Springer-Verlag, New York, 1990), Vol. 364.

- [2] M. Hjorth-Jensen, T. T. S. Kuo, and E. Osnes, *Phys. Rep.* **261**, 126 (1995), and references therein.
- [3] L. Coraggio, A. Covello, A. Gargano, N. Itaco and T.T.S. Kuo, *Prog. Part. Nucl. Phys.*, **62** (2009) 135, and references quoted therein.
- [4] B.A. Brown and B.H. Wildenthal, *Ann. Rev. Nucl. Part. Sci.* **38**, 29(1988).
- [5] B.A. Brown, W.A. Richter, *Phys. Rev. C* **74**, 0343150 (2006).
- [6] T.T.S. Kuo, S.Y. Lee and K.F. Ratcliff, *Nucl. Phys.* **A176** (1971) 172.
- [7] S.Y. Lee and K. Suzuki, *Phys. Lett.* **91B**, 173 (1980).
- [8] K. Suzuki and S.Y. Lee, *Prog. Theor. Phys.* **64**, 2091 (1980).
- [9] K. Suzuki, R. Okamoto, P.J. Ellis and T.T.S. Kuo, *Nucl. Phys.* **A567** (1994) 576.
- [10] E.M. Krenciglowa and T.T.S. Kuo, *Nucl. Phys.* **A235**, 171 (1974).
- [11] T.T.S. Kuo, F. Krmpotic, K. Suzuki and R. Okamoto, *Nucl. Phys.* **A582**, 205(1995).
- [12] R. Okamoto, K. Suzuki, H. Kumagai and S. Fujii, to be published in ‘Proceedings of the 10th International Spring Seminar on Nuclear Physics (May 21-25, Sur Mare Vietri, Italy, ed. by A. Covello)’; [nucl-th] arXiv:1011.1994v1.
- [13] L. Coraggio and N. Itaco, *Phys. Lett.* **B616**, 43 (2005).
- [14] S. K. Bogner, T. T. S. Kuo and L. Coraggio, *Nucl. Phys.* **A684**, (2001) 432.
- [15] S.K. Bogner, T.T.S. Kuo, L. Coraggio A. Covello, and N. Itaco, *Phys. Rev. C* **65**, 051301(R) (2002).
- [16] S. K. Bogner, T. T. S. Kuo, and A. Schwenk, *Phys. Rep.* **386**, 1 (2003).
- [17] D. R. Entem, R. Machleidt, and H. Witala, *Phys. Rev. C* **65**, 064005 (2002).
- [18] R. Machleidt, *Phys. Rev. C* **63**, 024001 (2001).
- [19] R. B. Wiringa, V. G. J. Stoks, and R. Schiavilla, *Phys. Rev. C* **51**, 38 (1995).
- [20] V. G. J. Stoks, R. A. M. Klomp, C. P. F. Terheggen, and J. J. de Swart, *Phys. Rev. C* **49**, 2950 (1994).
- [21] H. Dong, T.T.S. Kuo and J. W. Holt, preprint (May 2011, to be submitted to arXiv and PRC).
- [22] <http://www.nndc.bnl.gov/chart/>.
- [23] J.D. Holt, J. W. Holt, T. T. S. Kuo, G. E. Brown and S. K. Bogner, *Phys. Rev.* **C72**, 041304(R) (2005).